Computer Physics Communications 183 (2012) 2519–2527

Contents lists available at SciVerse ScienceDirect

Computer Physics Communications

journal homepage: www.elsevier.com/locate/cpc

Issues and challenges in orbital-free density functional calculations

V.V. Karasiev *, S.B. Trickey

Quantum Theory Project, Departments of Physics and of Chemistry, P.O. Box 118435, University of Florida, Gainesville FL 32611-8435, United States

ARTICLE INFO

Article history:
Received 3 October 2011
Received in revised form
4 June 2012
Accepted 30 June 2012
Available online 3 July 2012

Keywords:
Kinetic energy functional
Orbital-free density functional theory
Euler equation
Electronic structure

ABSTRACT

Solving the Euler equation which corresponds to the energy minimum of a density functional expressed in orbital-free form involves related but distinct computational challenges. One is the choice between all-electron and pseudopotential calculations and, if the latter, construction of the pseudopotential. Another is the stability, speed, and accuracy of solution algorithms. Underlying both is the fundamental issue of satisfactory quality of the approximate functionals (kinetic energy and exchange–correlation). We address both computational issues and illustrate them by some comparative performance testing of our recently developed modified-conjoint generalized gradient approximation kinetic energy functionals. Comparisons are given for atoms, diatomic molecules, and some simple solids.

1. Introduction

Investigation of orbital-free density functional theory (OF-DFT) [1–12], including development of approximate orbital-free kinetic energy (OFKE) functionals, has at least two motivations. One is simply the beguiling notion of direct realization of the content of the Hohenberg–Kohn theorem [13–17]. The other is practical, namely the possibility of eliminating the computational bottleneck of solving the Kohn–Sham (KS) eigenvalue equations, thereby dramatically broadening the applicability of Born–Oppenheimer molecular dynamics run with DFT electronic energies. The practical aspect is the main focus of the present work.

In OF-DFT, the total electronic energy of an N_e electron system is a functional of the electron density $n(\mathbf{r})$

$$E^{\text{OF-DFT}}[n] = T_s[n]s + E_{\text{Ne}}[n] + E_{\text{H}}[n] + E_{\text{xc}}[n] + E_{\text{NN}}, \tag{1}$$

where $T_s[n]$ is the KS (non-interacting) kinetic energy functional given explicitly as a density functional, $E_{\text{Ne}}[n]$ is the nuclear–electron interaction energy, $E_{\text{H}}[n]$ is the Hartree energy (classical electron–electron repulsion), $E_{\text{xc}}[n]$ is the exchange–correlation (XC) energy functional, and E_{NN} is the inter-nuclear repulsion energy. Minimization of the functional Eq. (1) gives a single Euler equation to be solved,

$$\frac{\delta T_s[n]}{\delta n(\mathbf{r})} + v_{\text{KS}}([n];\mathbf{r}) = \mu. \tag{2}$$

Here v_{KS} is the Kohn–Sham potential, $\delta(E_{\text{Ne}} + E_{\text{H}} + E_{\text{xc}})/\delta n$ and μ is the chemical potential. The ordinary KS equation has the same potential but requires solution for N_e or $N_e/2$ orbitals (in the all-electron, spin-polarized and non-spin-polarized cases respectively). Solution of the ordinary KS problem scales computationally as $\approx N_e^3$ in general, whereas solution of Eq. (2) should scale approximately linearly.

Practical implementation of OF-DFT requires approximation of both $T_s[n]$ and $E_{\text{xc}}[n]$. Simply because of their relative magnitudes, the quality of an OF-DFT calculation is dominated by the quality of the approximate T_s. There are two distinct classes of approximation in the literature, one-point functionals,

$$T_s[n] = \int t_s([n];\mathbf{r})d^3\mathbf{r} \tag{3}$$

and two-point functionals

$$T_s[n] = \int f_{1,s}([n];\mathbf{r})\chi(\mathbf{r},\mathbf{r}')f_{2,s}([n];\mathbf{r}')d^3\mathbf{r}d^3\mathbf{r}'. \tag{4}$$

Here $f_{1,s}$ and $f_{2,s}$ are weighting functionals and $\chi(\mathbf{r},\mathbf{r}')$ is a type of response function. For reasons of computational efficiency as well as conceptual simplicity (two-point functionals take the development out of the framework of an effective Kohn–Sham equation (see Eq. (8) below) unless an optimized effective potential [18] is used, itself an extra complication), we (and our collaborators) have focused exclusively on one-point functionals and do so here as well.

An interesting feature of the literature on developing approximate OFKE functionals, including our contributions with collaborators, is that there are more tests of approximate functionals using inputs from other sources (*e.g.* conventional KS calculations,

* Corresponding author. Tel.: +1 352 392 6976.
E-mail addresses: vkarasev@gmail.com, vkarasev@qtp.ufl.edu (V.V. Karasiev), trickey@qtp.ufl.edu (S.B. Trickey).

0010-4655/$ – see front matter © 2012 Elsevier B.V. All rights reserved.
doi:10.1016/j.cpc.2012.06.016

Hartree–Fock calculations, etc.) than tests by solving the Euler equation, (2). A side-effect is that comparatively little is known about the difficulty of solving that equation with approximations other than of the Thomas–Fermi kind (see below) and about the relative effectiveness of various solution techniques.

To frame that issue and the calculations reported here, it is useful to decompose the non-interacting KE functional into the von Weizsäcker contribution [19] plus a non-negative remainder, the Pauli term [20–23],

$$T_s[n] = T_W[n] + T_\theta[n], \quad T_\theta[n] \geq 0. \tag{5}$$

The von Weizsäcker functional (in Hartree atomic units) is

$$T_W[n] = \frac{1}{8}\int \frac{|\nabla n(\mathbf{r})|^2}{n(\mathbf{r})} d^3\mathbf{r} \equiv \int t_W([n];\mathbf{r}) d^3\mathbf{r}. \tag{6}$$

It is exact for one electron and for a two-electron singlet. From

$$\frac{\delta T_W[n]}{\delta n(\mathbf{r})} = \frac{1}{\sqrt{n(\mathbf{r})}}\left(-\frac{1}{2}\nabla^2\right)\sqrt{n(\mathbf{r})}, \tag{7}$$

the Euler equation Eq. (1) takes a Schrödinger-like form [23–25]

$$\left\{-\frac{1}{2}\nabla^2 + v_\theta([n];\mathbf{r}) + v_{KS}([n];\mathbf{r})\right\}\sqrt{n(\mathbf{r})} = \mu\sqrt{n(\mathbf{r})}. \tag{8}$$

Observe that, unlike familiar quantum mechanical eigenvalue problems, the "orbital" in Eq. (8) is normalized to N_e, not unity. Here v_θ is the Pauli potential,

$$v_\theta([n];\mathbf{r}) = \frac{\delta T_\theta[n]}{\delta n(\mathbf{r})}$$

$$v_\theta([n];\mathbf{r}) \geq 0. \tag{9}$$

Non-negativity of T_θ and v_θ has proved to be an important pair of constraints for OFKE functional development [9–11].

Eq. (8) resembles the ordinary KS equation, a fact that has led to contradictory statements about solution techniques. On the one hand, Ref. [25] declares that Eq. (8) "…can be solved iteratively to self-consistency by any Kohn–Sham computer program: just select the lowest eigenvalue. The solution is very simple and quick, for there is only *one* 'orbital' …". Ref. [26] makes precisely the contrary claim, at least in the context of the widely used Gaussian-type orbital (GTO) basis sets. Those authors expanded $\sqrt{n}$ in a GTO basis with coefficients c_i, with respect to which they minimized $\mathcal{L} := E^{\text{OF-DFT}}[n] - \mu N_e$. They state that "Due to the highly non-quadratic nature of the kinetic energy, the optimization of $\mathcal{L}$ is a nontrivial problem. The iterative self-consistent procedure used in Kohn–Sham calculations does not work, and we require more robust minimization techniques. Moreover, …first derivative methods such as conjugate gradient minimization and quasi-Newton search perform poorly, requiring many hundreds of iterations to achieve convergence". A related discussion and references to the few earlier papers on the issue is at p. 135 of Ref. [14]. This is one of the issues addressed in the present study.

2. Approximate kinetic energy functionals

To set the stage for another technical issue, we consider types of approximate one-point OFKE functionals next. For work on minimization involving two-point functionals, see Refs. [27,28] and references therein.

2.1. Thomas–Fermi type

Diverse approximate OFKE functionals can be written in the generic form

$$T_s[n] = T_W[n] + \lambda T_{TF}[n] + T_\Delta[n] \quad 0 \leq \lambda \leq 1. \tag{10}$$

The simplest local approximation for the KE is the Thomas–Fermi (TF) [29,30] functional

$$T_{TF}[n] \equiv \int t_{TF}([n];\mathbf{r})\, d^3\mathbf{r} = c_0 \int n^{5/3}(\mathbf{r})\, d^3\mathbf{r}$$

$$c_0 = \frac{3}{10}(3\pi^2)^{2/3} \tag{11}$$

alone. The approximation $T_\Delta = 0$ and $\lambda = 1$ is widely used in many OF-DFT applications (see Ref. [2] for discussion and references) despite its known deficiencies [31]. A related form, commonly called Thomas–Fermi–Dirac–von Weizsäcker theory, is a linear combination of T_{TF} with some fraction of T_W,

$$T_{TFvW,\alpha} = \alpha T_W + T_{TF}; \quad 0 \leq \alpha \leq 1 \tag{12}$$

along with the local Dirac exchange functional. Early reports of special self-consistent OF-DFT calculations mentioned above were for this model [26,32,33].

As an aside, there is an extensive literature of efforts to determine an optimal value of α in Eq. (12). Since the Pauli term decomposition, Eq. (5), provides both an exact lower bound on T_s and leads to the density Schrödinger equation, Eq. (8), that decomposition, and its elaboration Eq. (10), seems preferable to using $T_{TFvW,\alpha}$ and attempting to optimize α. But because $T_{TFvW,\alpha}$ is prevalent in the literature, we consider the numerical issues associated with it as well.

2.2. Generalized gradient approximation KE functionals

Generalized gradient approximations (GGA) are best known in DFT as improvements on the local approximation for E_{xc}. For either E_{xc} or T_s, a GGA is a truncation of the corresponding gradient expansion which is altered to meet relevant constraints and suppress unphysical behaviors. For the KE functional, a GGA can be written as

$$T_s^{GGA}[n] = \int t_{TF}([n];\mathbf{r}) F_t(s(\mathbf{r})) d^3\mathbf{r}, \tag{13}$$

where F_t is the kinetic energy enhancement factor. It is a function of the dimensionless reduced density gradient,

$$s \equiv \frac{|\nabla n|}{(2k_F)n} = \frac{1}{2(3\pi^2)^{1/3}}\frac{|\nabla n|}{n^{4/3}}. \tag{14}$$

Because $t_W = \frac{5}{3}s^2 t_{TF}$, the GGA Pauli term in Eq. (5) is

$$T_\theta^{GGA}[n] = \int t_{TF}([n];\mathbf{r}) F_\theta(s(\mathbf{r})) d^3\mathbf{r}$$

$$F_\theta(s) = F_t(s) - \frac{5}{3}s^2. \tag{15}$$

Ref. [10] showed that the KS KE of a molecular system is dominated by the behavior of F_θ over a relatively small range of s. For much of that range, Fig. 1 displays the Pauli enhancement factors for the functionals $T_{TFvW,\alpha}$, with $\alpha = 1, 1/9$ Eq. (12), the Tran–Wesolowski GGA [34] (PBE-TW), and the mcGGA functional (PBE2) of Ref. [9]. The latter two use the same enhancement factor form as the Perdew, Burke, and Ernzerhof (PBE) [35] GGA X functional, $F_x(s) = 1 + cs^2/(1 + as^2)$. In PBE-TW $F_t \propto F_{x,PBE}$ with parameters fitted to reproduce the kinetic energy of a small training set, an assumption called conjointness. PBE2 is a "modified conjoint" GGA (mcGGA) functional because the parameters in it were constrained to satisfy Pauli-term non-negativity; see Ref. [10] for details.

Observe in Fig. 1 that the PBE-TW and $T_{TFvW,\alpha=1/9}$ Pauli enhancement factors are almost identical, especially for small s. There, both have negative slope (with respect to s^2) which causes violation of v_θ non-negativity [10], recall Eq. (9). The common

Table 1
All-numerical and GTO results for the atoms H, Li, and Ne for the $T_{TFvW,\alpha=0,1}$ models with simple Slater exchange. Energies in Hartree a.u.

	$T_s = T_W$ numer.	$T_s = T_W$ GTO	$T_s = T_W + T_{TF}$ numer.	$T_s = T_W + T_{TF}$ GTO	$T_s = T_W + T_{TF}$[a]
H atom					
E_{tot}	−0.406534	−0.400737	−0.261827	−0.259969	−0.2618
T_s	0.406534	0.859699	0.261827	0.262042	–
T_θ	0.000	0.000	0.091034	0.090221	–
μ	−0.1943	−0.1764	−0.0715	−0.0696	−0.071
Li atom					
E_{tot}	−8.525825	−8.523413	−4.105425	−4.096347	−4.1054
T_s	8.525825	8.523126	4.105425	4.103660	–
T_θ	0.000	0.000	2.019249	2.009622	–
μ	−0.9575	−0.9526	−0.1306	−0.0.1365	−0.131
Ne atom					
E_{tot}	−274.68080	−274.652253	−85.734451	−85.730041	−85.7343
T_s	274.68080	274.664688	85.734438	85.728273	–
T_θ	0.000	0.000	54.352106	54.347495	–
μ	−7.0607	−7.0594	−0.1807	−0.1806	−0.181

[a] From Ref. [26].

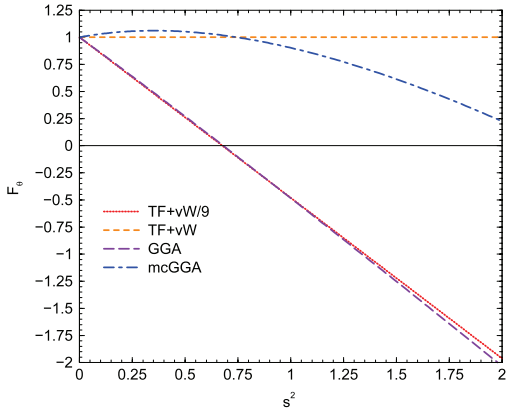

Fig. 1. Pauli term enhancement factors F_θ of OFKE functionals as a function of s^2. GGA denotes the Tran–Wesolowski functional, mcGGA denotes the PBE2 functional. See text for details.

property of the $T_{TFvW,\alpha=1}$ and PBE2 approximations is satisfaction of that non-negativity constraint. The low slope of the PBE2 enhancement factor at small values of s^2, $F_\theta^{PBE2}(s) \approx 1 + 0.3642s^2$, makes the enhancement factors for $T_{TFvW,\alpha=1}$ and T_{PBE2} close for $s < 1$. This comparison suggests that the results obtained with the PBE-TW KE functional should be close to those from $T_{TFvW,\alpha=1/9}$ and, similarly, the results from PBE2 should be close to those from $T_{TFvW,\alpha=1}$.

A technical problem common to these GGAs is that both $v_{\theta,\text{PBE-TW}}$ and $v_{\theta,\text{PBE2}}$ are singular at nuclear sites, the former negative, the latter positive. Numerical solution of the Euler equation Eq. (2) must address this problem, an issue to which we return below.

3. All-electron solutions of the OF-DFT Euler equation

As in ordinary KS calculations, solution of Eq. (8) can be either all-electron or via pseudopotentials. In this section, we consider all-electron solutions, by both GTO-basis and numerical grid techniques and address pseudopotentials in the subsequent section.

3.1. Atoms

To test the notion that any standard KS code can be used straightforwardly [25], we modified the GTO-basis code SOAtom to handle T_θ and v_θ as in Eqs. (5), (8) and (9). SOAtom, a part of the GTOFF suite [36,37], solves the KS equation in a Hermite Gaussian basis with analytical evaluation of all the matrix elements except for those involving XC. Those are done on a radial grid. We also modified the Laaksonen all-numerical diatomic molecular code [38] correspondingly. It is based on a prolate spheroidal grid.

Insofar as numerical stability is concerned, the results are quite clear. Even for $T_{TFvW,\alpha=1}$ with simple Slater exchange (*i.e.* TFvWD), the typical iterative SCF procedure is only marginally stable. The problem is worse in the GTO basis than in the grid-based calculation, at least in the specific sense that a simple SCF stabilization procedure (Pratt, *i.e.* linear mixing of a fraction of current iteration density and the rest from the preceding iteration) fails completely for many OF-DFT calculations. Ordinary KS calculations on the same atoms with the same simple stabilization scheme converge in a few iterations.

The lithium and carbon atoms are examples. For Li in a 9 s GTO basis in the SOAtom code, the pure TF form ($T_s = T_{TF}$, *i.e.*, Eq. (12) with $\alpha = 0$), the $T_\theta = T_{TF}$ form (Eq. (10) with $\lambda = 1$, $T_\Delta = 0$), and the $T_\theta = \lambda T_{TF}$ form (Eq. (10) with $T_\Delta = 0$) can be brought to numerical convergence but the mcGGA form $T_\theta = T_{mcGGA} - T_{vW}$ cannot. For the successes, more iterations by one to two orders of magnitude are required than for conventional KS and the numerical convergence is poor. One can get to fractional total energy errors of $10^{-4} \to 10^{-2}$ for lighter to heavier atoms respectively, but not much better. The contrast with conventional KS atomic calculations is stark: in them convergence to 10^{-6} is trivial to achieve.

Table 1 illustrates this point with comparison of numerical grid and GTO-basis results for $T_s = T_{vW}$ and $T_{vW} + T_{TF}$ with simple Slater exchange (Dirac exchange) on H, Li, and Ne. (The GTO calculations are with 9 s basis sets for H and Li, 13 s for Ne.) The two total energies for Li differ at the 1 mHa scale. Notice that the numerical-grid results match rather well with the values from Ref. [26], which were calculated with a direct minimization scheme, not a modified KS code. Ironically, a misbehavior of simple Slater exchange, namely that it satisfies the virial theorem in the form $E_{tot} = -T_s$ (which the exact E_{xc} does not), in this case highlights the convergence problem, especially in the GTO calculation.

Results for the carbon atom in the GTO basis, not shown in the table, are worse. The $T_{TFvW,\alpha=1/5}$ calculation with a 13 s basis cannot be brought to SCF convergence, even with tricks such as starting with full T_W and no T_{TF} contribution, then slowly scaling down the former while scaling up the latter. The corresponding standard KS calculation converges trivially.

For the numerical-grid calculations, SCF convergence is very slow compared to standard KS calculations, but reasonable results

Table 2
Self-consistent atomic total energies obtained from various OFKE functionals (Hartree a.u.) and simple Slater exchange.

	1/9 vW+TF[a]	1/9 vW+TF	1/5 vW+TF[a]	1/5 vW+TF	vW+TF[a]	vW+TF	GGA (PBE-TW)	mcGGA (PBE2)	KS[b]
H	−0.6664	−0.6664	−0.5666	−0.5666	−0.2618	−0.2618	−0.71	−0.32	−0.4065
He	−3.2228	−3.2228	−2.8184	−2.8184	−1.4775	−1.4775	−3.4	−1.5	−2.7236
Li	−8.2515	−8.2515	−7.3227	−7.3227	−4.1054	−4.1054	−8.6	−4.1	−7.1749
Be	−16.1631	−16.1631	−14.4841	−14.4841	−8.4922	−8.4922	−16.7	−8.4	−14.2233
B	−27.2876	−27.2876	−24.6284	−24.6284	−14.9258	−14.9259	−28.0	−14.6	−24.5275
C	−41.9052	−41.9053	−38.0332	−38.0332	−23.6568	−23.6569	−42.9	−23.0	−37.6863
N	−60.2622	−60.2623	−54.9428	−54.9429	−34.9084	−34.9084	−61.6	−33.9	−54.3977
O	−82.5798	−82.5799	−75.5765	−75.5765	−48.8831	−48.8832	−84.3	−47.3	−74.8076
F	−109.0592	−109.0594	−100.1345	100.1346	−65.7674	−65.7676	−111.1	−63.5	−99.4072
Ne	−139.8865	−139.8867	−128.8014	−128.8016	−85.7343	−85.7344	−142.3	−82.7	−127.4907

[a] From Ref. [26].
[b] Spin-restricted LDA (Slater exchange) calculation.

can be obtained. Table 2 shows total energies for the first row atoms obtained from numerical-grid self-consistent OF-DFT calculations with various OFKE approximations, again with Slater exchange. For TFvWD and $T_{TFvW,\alpha=1/5,1/9}$, comparison with the direct minimization of Ref. [26] (the first six columns of data) confirms that our calculations succeeded.

Note that the total energies from the TF+vW and mcGGA(PBE2) kinetic energy functionals are overestimated (as a consequence of overestimation of the KS KE). In contrast, all of the functionals with scaled von Weizsäcker contributions *underestimate* the KS KE, so that the resulting total energies are *below* the reference KS values. Such behavior is characteristic of a failure of N-representability in the KE functional [39]. Observe also that TF+1/9vW and GGA (PBE-TW) total energies are close to each other, though the functional forms differ.

Table 3 shows the effects of using the full LDA E_{xc}, in this case the VWN parameterization [40]. Unsurprisingly but reassuringly, inclusion of the C functional shifts the total energies downward without altering the trends.

These atomic results lead us to nuanced agreement with the claim of Ref. [26] and disagreement with the claim of Ref. [25]. The OF-DFT Euler equation is not, in general, solvable by simple modification of a standard GTO KS code (the norm for molecular calculations). Even a good all-numerical KS code is challenged to achieve solutions but can be made to succeed for isolated atoms. Realizing the computational speed-up potential of OF-DFT clearly depends on algorithms and implementations well suited for OF-DFT, even for one-point functionals.

3.2. Diatomic molecules

Numerical-grid solution of Eq. (8) for diatomic molecules, if possible, would yield two kinds of insight: numerical method behavior and the comparative behavior of $n(\mathbf{r})$ and $v_\theta(\mathbf{r})$ for different OFKE approximations. Though the difficulties of using a modified KS code are just as evident in this case, we have been able to achieve solutions for several light molecules.

Numerical requirements include extremely tight convergence tolerances on the eigenvalue μ and normalization (10^{-3} more stringent than normal KS calculations), much larger maximum distance cutoff (80–100 a.u. vs. normal KS 30–40 a.u.), and about a factor of five more points in both of the prolate spheroidal coordinates (roughly 1100×1300 points vs. the typical 200×300). Even so, the total energy convergence is mediocre for GGA and mcGGA functionals, about 0.01 Hartree at best. Convergence is better for the $T_{\mathrm{TFvW},\alpha}$ functionals, between 0.1 and 1 mHartree. This need for extreme measures to achieve limited-quality outcomes is an additional confirmation of the unsuitability of unmodified conventional KS schemes for solutions of the OF-DFT Euler equation.

The solutions nevertheless provide real comparative insight regarding different OFKE approximations. Fig. 2 compares the

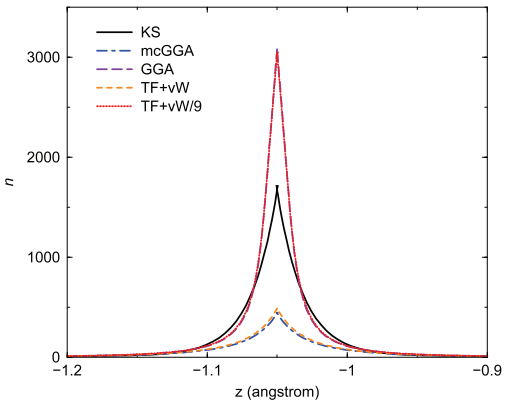

Fig. 2. All-electron self-consistent Kohn–Sham and OF-DFT electron densities plotted along the SiO molecule internuclear axis in the vicinity of the Si site. Si at (0, 0, −1.05) Å, O out of the picture at (0, 0,+1.05) Å. See text.

Table 3
OF-DFT self-consistent atomic total energies (Hartree a.u.) obtained from various kinetic energy functionals and VWN $E_{xc,LDA}$ with the numerical grid KS code.

	1/9 vW+TF	1/5 vW+TF	vW+TF	GGA (PBE-TW)	mcGGA (PBE2)	KS[a]
H	−0.7101	−0.6084	−0.2924	−0.76	−0.36	−0.4457
He	−3.3244	−2.9175	−1.5590	−3.5	−1.6	−2.8348
Li	−8.4175	−7.4860	−4.2469	−8.7	−4.2	−7.3352
Be	−16.3982	−14.7162	−8.6995	−16.9	−8.5	−14.4472
B	−27.5953	−24.9329	−15.2033	−28.4	−14.8	−24.3436
C	−42.2886	−38.4132	−24.0078	−43.3	−23.4	−37.4202
N	−60.7237	−55.4007	−35.3357	−62.1	−34.3	−54.0250
O	−83.1215	−76.1146	−49.3893	−84.8	−47.8	−74.4613
F	−109.6832	−100.7547	−66.3545	−111.7	−64.1	−99.0960
Ne	−140.5945	−129.5054	−86.4042	−143.1	−83.4	−128.2335

[a] Spin-restricted LDA calculation.

all-electron KS density ($E_{xc,LDA}$, VWN) around the Si site in SiO with the densities from $T_{GGA,PBE\text{-}TW}$ (the Tran–Wesolowski [34] GGA), $T_{mcGGA,PBE2}$ (the PBE2 mcGGA [9]), and $T_{TFvW,\alpha=1/9,1}$. These approximate functionals form pairs. $T_{GGA,PBE\text{-}TW}$ pairs with $T_{TFvW,\alpha=1/9}$, while $T_{TFvW,\alpha=1}$ pairs with $T_{mcGGA,PBE2}$. This pairing conforms to the expectations formed in considering the small-s behavior of the respective enhancement factors. The pairing also is interpretable directly from the near-nucleus repulsion or attraction behavior of the various approximations. $T_{GGA,PBE\text{-}TW}$ generates a v_θ with a spurious negative singularity near the nuclei, while $T_{TFvW,\alpha=1/9}$ drastically lowers the von Weizsäcker lower bound to T_s. Both lead to excess near-nucleus density. In contrast, $v_{\theta,mcGGA,PBE2}$ has spurious positive nuclear site singularities [10]. Near the nuclei, however, $v_{\theta,mcGGA,PBE2}$ and $v_{\theta,TFvW,\alpha=1}$ match quite well, as shown in Fig. 3. The result, shown in Fig. 2, is that these two functionals give rather close to the same density. Observe

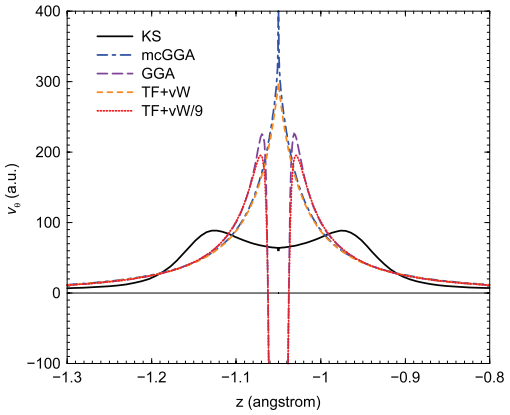

Fig. 3. Pauli potentials v_θ around the Si site in SiO from self-consistent all-electron Kohn–Sham and OF-DFT calculations with the PBE2 mcGGA, TW GGA, and $T_{TFvW,\alpha=1/9,1}$ OFKE functionals.

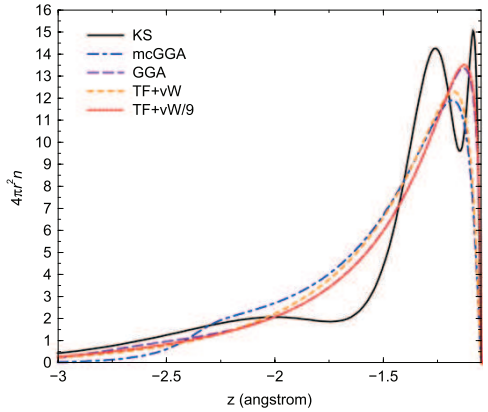

Fig. 4. All-electron self-consistent Kohn–Sham and OF-DFT electron densities near the Si site along the SiO molecular axis. These are scaled by the factor $4\pi\,(|z|-R/2)^2$, with $R = 2.10$ Å, the internuclear distance. This puts the origin of the scaling at the Si site $(0, 0, -1.05)$ Å. The O is out of the picture at $(0, 0, +1.05)$ Å.

that the behavior of v_θ in the vicinity of the nucleus for each of these approximate functionals differs dramatically from that of v_θ obtained by inversion of the standard KS scheme. It is that improper behavior which we believe causes the problems with convergence of standard KS codes used with approximate OFKE functionals. The positive near-nuclei singularities appear, in particular, to pose numerical problems.

Details of the density near the Si site are provided in Fig. 4. For purposes of display, the densities are weighted by a quasi-radial factor with origin at the Si site, $4\pi\,(|z| - R/2)^2$. The proper KS shell structure is missing, as is usual with single-point OFKE functionals. The more repulsive nature of the pair $T_{\mathrm{mcGGA,PBE2}}$ and $T_{TFvW,\alpha=1}$ compared to $T_{\mathrm{GGA,PBE\text{-}TW}}$ and $T_{TFvW,\alpha=1/9}$ also is evident. It is interesting that in the region $-2.5 < z < 2.0 T_{\mathrm{mcGGA,PBE2}}$ does give a weak mimicry of the outermost shell structure in T_s, unlike the other models. We are uncertain as to how reliable or useful this feature is.

Fig. 5 compares the behavior of $E^{\mathrm{OF-DFT}}[n]$ as a function of SiO bond length with standard KS results. One sees immediately that the GGA and mcGGA forms introduce numerical difficulties because of their dependence on the reduced density gradient s, Eq. (14). Clearly there is a grid interval-size problem which could be obviated by going to even denser grids but at obvious computational cost. The known failure of $T_{\mathrm{GGA,PBE\text{-}TW}}$ to give

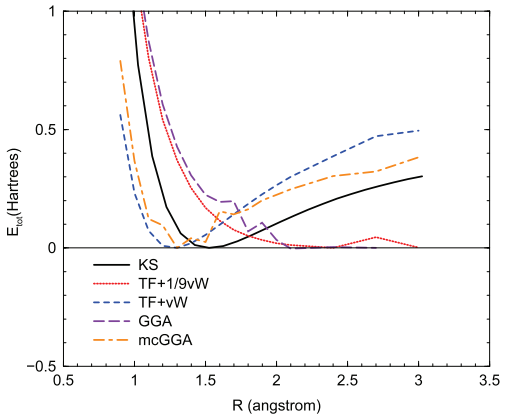

Fig. 5. Total energy of the SiO molecule as a function of bond length obtained from self-consistent all-electron Kohn–Sham and OF-DFT calculations with Thomas–Fermi, Tran–Wesolowski (GGA) and PBE2 (mcGGA) kinetic energy functionals. Kohn–Sham values are shown for comparison. Values are shifted to a common zero by 363.076 (KS), 386.339 (TF+vW/9), 250.529 (TF+vW), 83.902 (GGA) and 241.564 (mcGGA) Hartree a.u.

binding [9] is evident. $E_{TFvW,\alpha=1/9}$ apparently does not bind either, in keeping with the too-weakened lower bound just discussed. Full TFvWD and $E_{\mathrm{mcGGA,PBE2}}$ are fairly close, with the mcGGA being the best of the lot with respect to equilibrium bond length.

3.3. Simple analysis of the difficulty

The barrier to use of a standard KS code to solve Eq. (8) can be traced to the near-nucleus repulsion of v_θ. As displayed in Fig. 3, the exact v_θ is strongly repulsive in a fairly small region around the nuclear site and can have rather sharp structure within a radius of about 1 bohr of a nuclear site. In contrast, some simple approximations which are properly positive definite, including our mcGGA, actually are singular at the nuclei; again see Fig. 3. Such strong repulsion overwhelms the attractive v_{xc}. That figure also shows that some approximations deliver Pauli potentials with negative nuclear-site singularities. We consider that case below. First, however, the simplest example will suffice to illustrate the problem with properly positive v_θ. Pick $T_\theta = T_{\mathrm{TF}}$, Eq. (11), and E_{xc} to be simplest Slater exchange:

$$E_{\mathrm{xc}} = c_{\mathrm{x}} \int n^{4/3}(\mathbf{r}) d^3\mathbf{r}$$

$$c_{\mathrm{x}} = -\frac{3}{4}\left(\frac{3}{\pi}\right)^{1/3}. \tag{16}$$

Then in Eq. (8), the potentials become

$$v_\theta = \frac{1}{2}(3\pi^2)^{2/3} n^{2/3}(\mathbf{r})$$
$$v_{\mathrm{KS}} = v_{\mathrm{H}} + v_{\mathrm{Ne}} + v_{\mathrm{xc}}$$
$$v_{\mathrm{xc}} = -\left(\frac{3}{\pi}\right)^{1/3} n^{1/3}(\mathbf{r}). \tag{17}$$

A hydrogen-like density,

$$n_{\mathrm{H}}(\mathbf{r}) := \frac{N_e^4}{\pi} \exp(-2N_e r), \tag{18}$$

obeys the Kato cusp condition near the nucleus [16,41–44], hence is useful for testing. At the nucleus, this density yields the ratio of potentials

$$\frac{v_{\mathrm{xc}}(0) + v_\theta(0)}{|v_{\mathrm{xc}}(0)|} = -1 + 3.318004 N_e^{4/3}. \tag{19}$$

For $N_e = 6$, this ratio is already 35.2. By $N_e = 10$ it is 70.5. Additional simple calculations with the potential which appears in Eq. (8) without the positive Hartree contribution, that is $v_{\rm Ne}(r) + v_\theta(r) + v_{\rm xc}(r)$, illustrate the point. At small r with $N_e = 6$, that potential becomes positive for $r > 0.028$ Bohr. For $N_e = 10$ it is positive for $r > 0.011$ Bohr. These little exercises illustrate why the use of an ordinary KS code becomes so difficult. Such peculiar behavior is quite different from what is encountered in the ordinary KS problem.

From the perspective of numerical stability, the case of a v_θ which has a spurious negative singularity near each nuclear site, *e.g.* PBE-TW, is at least as bad if not worse. As a site is approached, such potentials first are increasingly repulsive, then plunge abruptly into the negative singularity; see Fig. 3.

4. Pseudo-potential solutions of the OF-DFT Euler equation

Having demonstrated the difficulties with solving the OF-DFT Euler–Lagrange problem with a modified KS eigenvalue code, we turn to the use of direct Euler–Lagrange minimization. The specific objective is to exploit the numerical methodology in the Profess code [27,28]. Written originally for use with two-point functionals, Profess performs OF-DFT calculations by minimization of the Euler–Lagrange equation as a functional of $n(\mathbf{r})$ under periodic boundary conditions. It uses a numerical 3D mesh and FFTs. As published, the code includes the TF, vW, and TFvW, α functionals as well as the Wang–Teter (WT) [45], and Wang–Govind–Carter (WGC) [46] OFKE functionals. The PZ and PBE $E_{\rm xc}$ functionals are implemented in Profess. For this study, we added the Tran–Wesolowski GGA [34] and our PBE2 mcGGA [9] OFKE functionals.

As is the case with standard KS calculations done in a plane-wave basis, Profess relies upon pseudopotential (PP) techniques to screen the nuclear–electron potential cusp and exclude chemically inactive core states. Though OF-DFT has no problem with core states and the density (and its square root) is a comparatively unstructured, smooth function, regularization of the nuclear–electron interaction singularity still is a requisite for an efficient implementation.

High-quality pseudopotentials developed for conventional KS calculations generally are non-local, in the specific sense that they contain projection operators which provide different potentials for different orbital angular momenta. That explicit orbital dependence makes non-local pseudopotentials (NLPP) inapplicable in OF-DFT calculations. Instead, local pseudopotentials (LPP), *i.e.*, of the form of a simple multiplicative operator which is the same for all orbitals, must be developed. Profess requires an LPP in real or reciprocal space as input. Observe that this limitation to local form is an additional approximation, over and beyond the PP itself, which has accuracy limitation implications for both conventional, orbital-based KS or OF-DFT implementations.

In addition to their simplicity, there is a formal advantage of LPPs which is at least of peripheral interest here. Calculations with local PPs are within the framework of the standard KS scheme, which assumes a local effective potential. The NLPP case obviously does not meet that assumption. Although the Hohenberg–Kohn theorem has been extended to the case of a non-local external potential [47], the exchange–correlation energy in that case becomes a functional of the one-particle reduced density matrix instead of a functional $n(\mathbf{r})$ alone.

Many methods have been proposed to develop LPPs. Among them we mention (i) empirical (or model) LPPs, for example in Refs. [48–52]; (ii) local potentials obtained from non-local ones, for example, by use of just one l-channel from an NLPP as an LPP (for example, Ref. [53]); (iii) LPPs constrained to reproduce atomic properties, eigenvalues, or pseudo-density, etc., which follow from a (presumably superior) NLPP (for example, Ref. [54]), and finally (iv) local PPs derived to reproduce some bulk property values, either experimental or those predicted by NLPP calculations [54–56].

4.1. Local pseudopotentials for OF-DFT calculations

4.1.1. Development

Some time ago, an iterative procedure was developed [57,58] to solve the inverse problem of determining the KS effective potential $v_{\rm KS}(\mathbf{r})$ from a given density $n(\mathbf{r})$. Subsequently, we [59] introduced and tested an improvement. In the case of Li, however, both versions share a problem. For a single valence orbital (singly or doubly occupied) the solution of the inverse problem is trivial and known. The local pseudopotential is equal to the s-channel of the NLPP, $v_{local}(r) = v_{l=0}(r)$. Hence the LPP contains no information about the $l > 0$ channels of the NLPP. Those channels are critical in crystalline binding.

Therefore, to include information about all l channels of the reference NLPP, we consider a sort of normalized linear combination of l components of that NLPP,

$$v_{l_{max}}(\mathbf{r}) = \sum_{l=0}^{l_{max}} c_l v_l(\mathbf{r}) \Big/ \sum_{l=0}^{l_{max}} c_l \tag{20}$$

where the parameters $\{c_l\}$ are to be adjusted to fit selected equilibrium bulk material properties calculated with the reference KS method. This particular method of LPP generation amounts to a mixture of methods (ii) and (iv) described at the outset of this section.

In the present case, we simply took the bcc Li lattice constant as predicted by a standard KS calculation with PBE [35] $E_{\rm xc}$, and the plane wave (PW) basis set (see Table 4, namely $a = 3.44$ Å). Components of the Troullier–Martins norm-conserving NLPP were used in Eq. (20). For generation of the NLPP with PBE XC, we took the core radius to be 2.45 a.u. The parameters $\{c_l\}$ in Eq. (20), for the s, p, and d channels respectively, were determined by constraining a KS calculation with the LPP equation (20) to reproduce the reference optimized bcc Li lattice constant value. Those KS calculations were done with PBE XC in the Siesta code [60] and a DZP numerical atomic orbital (NAO) basis set. The optimized parameter values are $c_0 = 0.69$, $c_1 = 0.34$, $c_2 = 0.10$. We designate this LPP as $v_{\rm GGA,spd1}$. To generate the LDA local LPP, $v_{\rm LDA,spd1}$ for the Perdew–Zunger [61] LDA XC functional, components of the LDA NLPP and the same set of channel-mixing parameters were used in Eq. (20).

An alternative LPP form which we also studied is a modification of the potential proposed by Heine and Abarenkov [50], Goodwin et al. [51]. In real space, the Heine–Abarenkov model potential is

$$v_{\rm mod}(r) = \begin{cases} -A, & r < r_c \\ -Z/r, & r \geq r_c \end{cases} \tag{21}$$

where A is a constant, r_c is the core radius, and Z is the core charge. The model potential in reciprocal space is given by

$$v_{\rm mod}(q) = \frac{-4\pi}{\Omega q^2}[(Z - Ar_c)\cos(qr_c) + (A/q)\sin(qr_c)], \tag{22}$$

where Ω is the unit cell volume. In Ref. [51], this potential was multiplied by a smoothed step function $f(q) = \exp[(-q/q_c)^6]$ to reduce spurious oscillations in $v_{\rm mod}(q)$ and to ensure rapid decay of $v_{\rm mod}(q)$ at large wave-vectors. Those oscillations are caused by the discontinuity of the real-space potential at the core radius. Here, the parameter q_c was chosen as suggested in Ref. [51], namely, to equal the second zero position of $v_{\rm mod}(q)$.

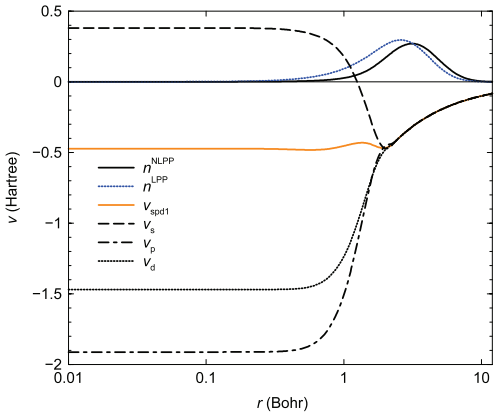

Fig. 6. Real space pseudopotentials for Li: local $v_{GGA,spd1}$, and different l-components of the non-local Troullier–Martin (TM) pseudopotential. Pseudodensities generated with local and non-local PPs are shown for comparison.

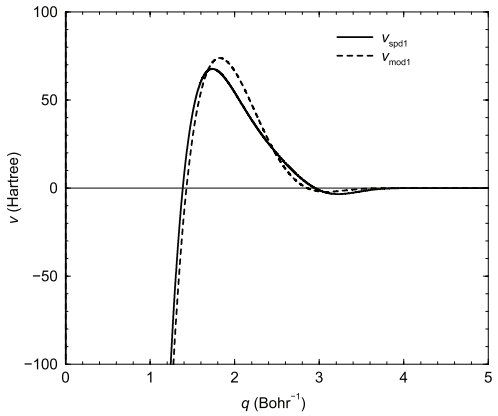

Fig. 7. Reciprocal space local pseudopotentials for Li: $v_{GGA,spd1}$ and $v_{GGA,mod1}$.

To obtain counterparts of the local potentials $v_{GGA,spd1}$ and $v_{LDA,spd1}$, Eq. (21) in the simple modified Heine–Abarenkov model form, the two parameters, A and r_c, were determined by minimization of $\int d\mathbf{r}|v_{spd1}(\mathbf{r}) - v_{mod1}(\mathbf{r})|^2$. This yields $A = 0.45499$ Hartree, $r_c = 2.2261$ Bohr, $g_c = 2.86$ Bohr^{-1} for $v_{GGA,mod1}$ and $A = 0.45376$ Hartree, $r_c = 1.8818$ Bohr, $g_c = 2.94$ Bohr^{-1} for $v_{LDA,mod1}$. The local potentials $v_{GGA,spd1}$ and $v_{LDA,spd1}$ in reciprocal space are multiplied by the same smoothed step function $f(q)$ with q_c values equal to 2.95 and 3.25 Bohr^{-1} respectively.

Fig. 6 shows the $v_{GGA,spd1}$ LPP in real space in comparison with the NLPP l channels, along with the two pseudodensities which result. Fig. 7 shows the $v_{GGA,spd1}$ and $v_{GGA,mod1}$ LPPs in reciprocal space.

4.1.2. KS tests of local pseudopotentials

Kohn–Sham calculations with the LPPs were performed using the Abinit PW code [62] with PZ and PBE exchange–correlation functionals. We also used Siesta with the same exchange–correlation functionals and a $2s^2 2p^2$ numerical atomic orbital basis set (8 NAO per atom). Table 4 shows the equilibrium lattice constants and bulk moduli for the various LPPs. Those results are compared to the Kohn–Sham calculations performed with the non-local projector augmented wave (PAW) scheme (as implemented in Vasp [63] and Abinit) and TM norm-conserving pseudopotentials with core correction [64]. The lattice constants and bulk moduli reported in Table 4 were obtained by fitting the calculated total energies per cell to the stabilized jellium model equation of state (SJEOS, [66]). All the local PPs reproduce the PAW results rather closely for both lattice constant and bulk modulus. The bulk moduli calculated using NAO orbitals and norm conserving TM pseudopotentials are slightly larger than the PAW plane wave results.

Table 4
Kohn–Sham lattice constant (Å) and bulk modulus (GPa) for bcc Li calculated using Vasp PW PAW schemes, Abinit PW PAW and local pseudopotentials, Siesta non-local Troullier–Martins [64,65] and local pseudopotentials. Orbital-free calculations used $T_{mcGGA,PBE2}$, $T_{TFvW,\alpha=1}$, $T_{GGA,PBE-TW}$, and $T_{TFvW,\alpha=1/9}$ kinetic energy functionals in combination with $E_{xc,LDA,PZ}$ and $E_{xc,GGA,PBE}$ with local pseudopotentials $v_{LDA,spd1}$, $v_{GGA,spd1}$, $v_{LDA,mod1}$ and $v_{GGA,mod1}$. Conventional KS calculations were done with a two-atom unit cell and $7 \times 7 \times 7$ (Vasp and Siesta) or $9 \times 9 \times 9$ (Abinit) **k**-mesh. The Siesta basis set was $2s^2 2p^2$ (8 NAO per atom). Orbital-free calculations used a 128-atom supercell.

Method	PP	LDA		GGA	
		a	B	a	B
Kohn–Sham					
PW (Vasp)	PAW	3.37	15.0	3.45	13.7
PW (Abinit)	PAW	3.37	15.1	3.44	13.9
NAO (Siesta)	TM	3.37	15.6	3.44	14.3
Kohn–Sham					
PW (Abinit)	spd1[a]	3.37	14.8	3.44	13.8
NAO (Siesta)	spd1[a]	3.38	14.9	3.45	13.9
Kohn–Sham					
PW (Abinit)	mod1[b]	3.37	14.8	3.44	13.9
NAO (Siesta)	mod1[b]	3.38	14.9	3.44	13.9
OF-DFT					
mcGGA	spd1[c]	3.37	16.2	3.43	15.4
TF+vW	spd1[c]	3.37	16.0	3.43	15.2
GGA	spd1[c]	3.37	11.8	3.46	11.8
TF+1/9vW	spd1[c]	3.37	11.4	3.46	11.4
OF-DFT					
mcGGA	mod1[d]	3.36	16.2	3.43	15.2
TF+vW	mod1[d]	3.37	15.9	3.43	14.9
GGA	mod1[d]	3.42	10.8	3.49	10.1
TF+1/9vW	mod1[d]	3.42	10.3	3.49	9.5

[a] Real space potential defined by Eq. (20) (see text for details).
[b] Real space potential defined by Eq. (21) (see text for details).
[c] Reciprocal space potential defined by Fourier–Bessel transform of local potential Eq. (20) and multiplied by $f(q)$ function (see text for details).
[d] Reciprocal space potential defined by Eq. (22) multiplied by $f(q)$ function (see text for details).

As a check against an all-electron localized-orbital calculation, we did high-quality GTO-basis KS calculations (10s6p3d basis) with the GTOFF code [37]. For $E_{xc,PZ}$ and $E_{xc,PBE}$, we obtained optimized bcc Li lattice parameters of 3.360 and 3.435 Å, respectively, essentially the same as from the Siesta NAO and plane wave PAW calculations.

4.2. Pseudopotential OF-DFT tests

4.2.1. OF-DFT comparison for bcc Li

For the OF-DFT bcc Li studies, we used a 128-atom supercell in Profess with the v_{spd1}, v_{mod1} LPPs just described and both $E_{xc,LDA}$ and $E_{xc,GGA}$. We did the Profess calculations for the T_{TF}, $T_{TFvW,\alpha=1,1/9}$, $T_{GGA,PBE-TW}$, and $T_{mcGGA,PBE2}$ functionals. The computed E_{tot}/atom values are plotted as a function of bcc lattice constant in Fig. 8.

One sees that, as might be expected, the pure TF+XC model fails to bind. The pairing of other functionals, which we have discussed already, reappears. $T_{TFvW,\alpha=1}$ pairs with $T_{mcGGA,PBE2}$, and $T_{TFvW,\alpha=1/9}$ pairs with $T_{GGA,PBE-TW}$. The former pair gives a better description of both the lattice constant and bulk modulus than the latter pair. The computed equilibrium lattice constants and bulk moduli are shown in Table 4.

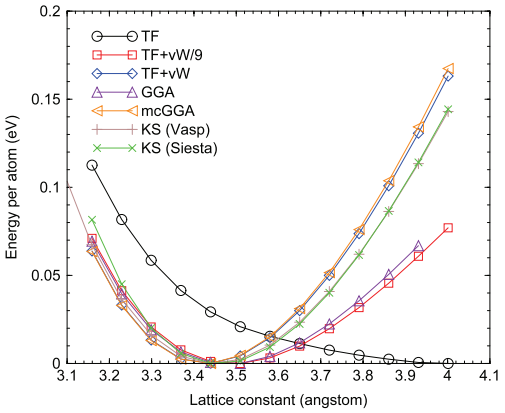

Fig. 8. Energy per atom vs. lattice constant for bulk bcc Li. OF-DFT results for T_{TF}, $T_{\mathrm{TFvW},\alpha}$, $T_{\mathrm{GGA,PBE\text{-}TW}}$, and $T_{\mathrm{mcGGA,PBE2}}$ compared to the KS values. OF-DFT calculations with 128-atom supercell, $v_{\mathrm{GGA,mod1}}$ LPP, and $E_{\mathrm{xc,GGA,PBE}}$. KS calculations two-atom unit cell with non-local PAW PBE pseudopotentials (VASP) and with Troullier–Martin PPs with PBE exchange–correlation, $2s^2 2p^2$ basis set (8 NAO per atom) (SIESTA).

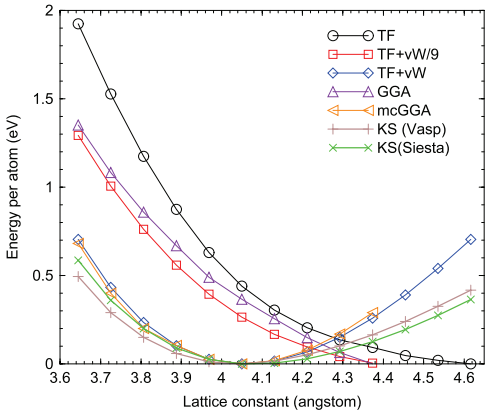

Fig. 9. As in Fig. 8 for bulk Al but with a four-atom supercell. SIESTA calculations performed with standard DZP basis set. The Goodwin et al. [51] local model pseudopotential was used in the orbital-free calculations. See text.

The equilibrium lattice constants predicted by the OF-DFT calculations with v_{spd1} LPPs agree well with the KS PAW results. When the v_{mod1} model pseudopotential is used, the lattice constant from the OF-DFT calculations with $T_{\mathrm{GGA,PBE\text{-}TW}}$ and $T_{TFvW,\alpha=1,1/9}$ is an over-estimate of about 1% for both LDA and GGA XC functionals. This pair of OFKE functionals also predicts low bulk modulus values, again for both LDA and GGA XC cases. The mcGGA and TF+vW KE functionals do very well for the lattice parameter and slightly overestimate the bulk modulus value.

4.2.2. OF-DFT comparison for fcc Al

The utility of existing LPPs for OF-DFT calculations obviously is a pertinent issue. To explore that, we considered bulk Al. The model LPP in the form of Eq. (22) with parameters from Goodwin et al. [51] was used in OF-DFT calculations. As before, this was done with the five OF-KE functionals, but here only in combination with the PBE GGA XC functional. Fig. 9 shows PROFESS results for a four-atom fcc cell compared with conventional KS results obtained with VASP in the same cell with a $5 \times 5 \times 5$ **k**-mesh calculation. The GGA and mcGGA KE functionals introduce numerical instability at expanded geometry. Aside from that, one again observes the same pairing of KE functionals as before. The $T_{\mathrm{GGA,PBE\text{-}TW}}$ and $T_{TFvW,\alpha=1/9}$ functionals do not produce detectable minima. The $T_{\mathrm{mcGGA,PBE2}}$ and $T_{TFvW,\alpha=1}$ pair predict equilibrium lattice constants ($a = 4.05$ and 4.06 Å correspondingly), very close to the KS results ($a = 4.05$ and 4.09 Å for PAW VASP and NAO DZP SIESTA calculations respectively). However, the shape of the two OF-DFT energy curves differs perceptibly from the KS results. In particular, the OF-DFT functionals predict a softer solid.

5. Summary discussion

Several clear results emerge from this study. First, use of standard KS codes to solve the OF-DFT Euler equation as a modified KS eigenvalue problem is problematic at best. At least for the all-electron case, it seems implausible as a productive route to routine OF-DFT calculations. One could speculate that a better-behaved one-point approximate OFKE functional than mcGGA might not be such a challenge to standard KS algorithms. The repulsive nature of even the exact v_θ (recall Fig. 3) makes that outcome seem rather doubtful.

Second, even if a particular approximate one-point OFKE functional has singular behavior, it is possible that such a functional can deliver physically realistic results. Those results can be obtained with a sufficiently refined direct Euler–Lagrange solution of the effective KS equation, Eq. (2). Thus, we are able to extract useful, self-consistent solutions for the recently developed simple mcGGA OFKE functional as well as the Tran–Wesolowski GGA. These solutions enable understanding of the consequence of the singular behavior of their respective Pauli potentials. The Tran–Wesolowski GGA has attractive singularities which cause strong overestimates of the self-consistent density near the nuclear sites. In contrast, the properly positive mcGGA OFKE Pauli potential has positive singularities near the nuclei and the density is underestimated there.

Third, we have presented a procedure for developing a local pseudopotential for OF-DFT calculations by doing a multi-channel weighting of a corresponding non-local pseudopotential. The weighting is determined by KS calculations with the LPP such that the equilibrium non-LPP lattice parameter is reproduced. We showed that this yields a very good LPP. A remaining challenge for the OF-DFT agenda is to construct a good LPP from an existing non-LPP without appeal to any bulk or aggregate system KS calculations.

Fourth, once a suitable local pseudopotential procedure is defined, the progress made on computational solution of the minimization problem for two-point OFKE approximations can be appropriated directly for use with one-point OFKE approximations. Even so, we do observe numerical instabilities in the case of the mcGGA and GGA OFKE functionals.

Acknowledgments

We acknowledge with thanks informative conversations with Frank Harris, Travis Sjostrom, and Jim Dufty. This work was supported in part by the US Dept. of Energy TMS program, grant DE-SC0002139.

References

[1] Y.A. Wang, E.A. Carter, in: S.D. Schwartz (Ed.), Theoretical Methods in Condensed Phase Chemistry, Kluwer, NY, 2000, p. 117. (Chapter 5) and references therein.
[2] E.V. Ludeña, V.V. Karasiev, in: K.D. Sen (Ed.), Reviews of Modern Quantum Chemistry: A Celebration of the Contributions of Robert Parr, World Scientific, Singapore, 2002, p. 612.
[3] B.-J. Zhou, Y.A. Wang, J. Chem. Phys. 124 (2006) 081107.

[4] D. García-Aldea, J.E. Alvarellos, Phys. Rev. A 77 (2008) 022502; J. Chem. Phys. 127 (2007) 144109 and references in both.
[5] J.P. Perdew, L.A. Constantin, Phys. Rev. B 75 (2007) 155109.
[6] C.J. Garcia-Cervera, Commun. Computat. Phys. 3 (2008) 968.
[7] L.M. Ghiringhelli, L. Delle Site, Phys. Rev. B 77 (2008) 073104.
[8] W. Eek, S. Nordholm, Theoret. Chem. Accounts 115 (2006) 266.
[9] V.V. Karasiev, S.B. Trickey, F.E. Harris, J. Comp.-Aided Mater. Des. 13 (2006) 111.
[10] V.V. Karasiev, R.S. Jones, S.B. Trickey, F.E. Harris, Phys. Rev. B 80 (2009) 245120.
[11] S.B. Trickey, V.V. Karasiev, R.S. Jones, Int. J. Quantum Chem. 109 (2009) 2943.
[12] C. Huang, E.A. Carter, Phys. Rev. B 81 (2010) 045206. [15 pp].
[13] P. Hohenberg, W. Kohn, Phys. Rev. 136 (1964) B864.
[14] R.G. Parr, W. Yang, Density Functional Theory of Atoms and Molecules, Oxford, New York, 1989.
[15] R.M. Dreizler, E.K.U. Gross, Density Functional Theory, Springer-Verlag, Berlin, 1990.
[16] E.S. Kryachko, E.V. Ludeña, Energy Density Functional Theory of Many-Electron Systems, Kluwer, Dordrecht, 1990.
[17] H. Eschrig, The Fundamentals of Density Functional Theory, Teubner, Stuttgart, 1996.
[18] J.D. Talman, W.F. Shadwick, Phys. Rev. A 14 (1976) 36;
O. Gritsenko, R. van Leeuwen, E. van Lenthe, E.J. Baerends, Phys. Rev. A 51 (1995) 1944;
S. Ivanov, S. Hirata, R.J. Bartlett, Phys. Rev. Lett. 83 (1999) 5455;
A. Görling, Phys. Rev. Lett. 83 (1999) 5459.
[19] C.F. von Weizsäcker, Z. Phys. 96 (1935) 431.
[20] Y. Tal, R.F.W. Bader, Int. J. Quantum Chem. S12 (1978) 153.
[21] L.J. Bartolotti, P.K. Acharya, J. Chem. Phys. 77 (1982) 4576.
[22] J.E. Harriman, in: R. Erdahl, V.H. Smith Jr. (Eds.), Density Matrices and Density Functionals, D. Reidel, Dordrecht, 1987, p. 359.
[23] M. Levy, H. Ou-Yang, Phys. Rev. A 38 (1988) 625.
[24] B.M. Deb, S.K. Ghosh, Int. J. Quantum Chem. 23 (1983) 1.
[25] M. Levy, J.P. Perdew, V. Sahni, Phys. Rev. A 30 (1984) 2745 and references therein.
[26] G. Kin-Lic Chan, A.J. Cohen, N.C. Handy, J. Chem. Phys. 114 (2001) 631.
[27] G.S. Ho, V.L. Lignères, E.A. Carter, Comput. Phys. Commun. 179 (2008) 839.
[28] L. Hung, C. Huang, I. Shin, G.S. Ho, V.L. Lignères, E.A. Carter, Comput. Phys. Commun. 181 (2010) 2208.
[29] L.H. Thomas, Proc. Cambridge Phil. Soc. 23 (1927) 542.
[30] E. Fermi, Atti Accad. Nazl. Lincei 6 (1927) 602.
[31] E.H. Lieb, Rev. Mod. Phys. 53 (1981) 603.
[32] Y. Tomishima, K. Yonei, J. Phys. Soc. Jpn. 21 (1966) 142.
[33] W. Yang, Phys. Rev. A 34 (1986) 4575.
[34] F. Tran, T.A. Wesolowski, Int. J. Quantum Chem. 89 (2002) 441.
[35] J.P. Perdew, K. Burke, M. Ernzerhof, Phys. Rev. Lett. 77 (1996) 3865; Phys. Rev. Lett. 78 (1997) 1396. (erratum).
[36] J.C. Boettger, Phys. Rev. B 57 (1998) 8743.
[37] S.B. Trickey, J.A. Alford, J.C. Boettger, in: J. Leszczynski (Ed.), Computational Materials Science, in: Theoretical and Computational Chemistry, vol. 15, Elsevier, Amsterdam, 2004, pp. 171–228.
[38] J. Kobus, L. Laaksonen, D. Sundholm, Comput. Phys. Commun. 98 (1996) 346.
[39] P.W. Ayers, S. Liu, Phys. Rev. A 75 (2007) 022514.
[40] S.H. Vosko, L. Wilk, M. Nusair, Can. J. Phys. 58 (1980) 1200.
[41] T. Kato, Commun. Pure Appl. Math. 10 (1957) 151.
[42] W.A. Bingel, Z. Naturforschung A 18 (1963) 1249.
[43] R.T. Pack, W.B. Brown, J. Chem. Phys. 45 (1966) 556.
[44] N.H. March, I.A. Howard, A. Holas, P. Senet, V.E. Van Doren, Phys. Rev. A 63 (2000) 012520.
[45] L.-W. Wang, M.P. Teter, Phys. Rev. B 45 (1992) 13196.
[46] Y.A. Wang, N. Govind, E.A. Carter, Phys. Rev. B 58 (1998) 13465.
[47] T.L. Gilbert, Phys. Rev. B 12 (1975) 2111.
[48] R.W. Shaw, Phys. Rev. 174 (1968) 769.
[49] W.C. Topp, J.J. Hopfield, Phys. Rev. B 7 (1973) 1295.
[50] V. Heine, I.V. Abarenkov, Phil. Mag. 9 (1964) 451.
[51] L. Goodwin, R.J. Needs, V. Heine, J. Phys.: Condens. Matter 2 (1990) 351.
[52] C. Fiolhais, J.P. Perdew, S.Q. Armster, J.M. MacLaren, M. Brajczewska, Phys. Rev. B 51 (1995) 14001.
[53] B.J. Costa Cabral, J.L. Martins, Phys. Rev. B 51 (1995) 872.
[54] B. Zhou, Y.A. Wang, E.A. Carter, Phys. Rev. B 69 (2004) 12509.
[55] S. Watson, B.J. Jesson, E.A. Carter, P.A. Madden, Europhys. Lett. 41 (1998) 37.
[56] C. Huang, E.A. Carter, Phys. Chem. Chem. Phys. 10 (2008) 7109.
[57] R. van Leeuwen, E.J. Baerends, Phys. Rev. A 49 (1994) 2421.
[58] O.V. Gritsenko, R. van Leeuwen, E.J. Baerends, Phys. Rev. A 52 (1995) 1870.
[59] Iterative Procedure to Determine Kohn–Sham Potentials from a Given Density: Application to All-electron and Pseudo-densities, V.V. Karasiev, S.B. Trickey, and F.E. Harris, (2007, unpublished).
[60] Spanish Initiative for Electronic Simulations with Thousands of Atoms (SIESTA); Version 2.0. See also J.M. Soler, E. Artacho, J.D. Gale, A. García, J. Junquera, P. Ordejón, D. Sánchez-Portal, J. Phys.: Condens. Matter 14 (2002) 2745. http://www.uam.es/departamentos/ciencias/fismateriac/siesta/.
[61] J.P. Perdew, A. Zunger, Phys. Rev. B 23 (1981) 5048.
[62] X. Gonze, B. Amadon, P.-M. Anglade, J.-M. Beuken, F. Bottin, P. Boulanger, F. Bruneval, D. Caliste, R. Caracas, M. Cote, T. Deutsch, L. Genovese, Ph. Ghosez, M. Giantomassi, S. Goedecker, D.R. Hamann, P. Hermet, F. Jollet, G. Jomard, S. Leroux, M. Mancini, S. Mazevet, M.J.T. Oliveira, G. Onida, Y. Pouillon, T. Rangel, G.-M. Rignanese, D. Sangalli, R. Shaltaf, M. Torrent, M.J. Verstraete, G. Zerah, J.W. Zwanziger, Computer Phys. Commun. 180 (2009) 2582;
X. Gonze, G.-M. Rignanese, M. Verstraete, J.-M. Beuken, Y. Pouillon, R. Caracas, F. Jollet, M. Torrent, G. Zerah, M. Mikami, Ph. Ghosez, M. Veithen, J.-Y. Raty, V. Olevano, F. Bruneval, L. Reining, R. Godby, G. Onida, D.R. Hamann, D.C. Allan, Zeit. Kristallogr. 220 (2005) 558.
[63] Vienna *ab initio* simulation package (VASP, Version 4.6. See also G. Kresse, J. Furthmüller, Comput. Mater. Sci. 6 (1996) 4136. http://cms.mpi.univie.ac.at/vasp/.
[64] Pseudopotentials are taken from the Siesta repository of translated norm-conserving Troullier–Martins pseudopotentials from the Fritz–Haber-Institute.
[65] N. Troullier, J.L. Martins, Phys. Rev. B 43 (1991) 1993.
[66] A.B. Alchagirov, J.P. Perdew, J.C. Boettger, R.C. Albers, C. Fiolhais, Phys. Rev. B 63 (2001) 224115.